The cytoskeleton as a soft glassy material

Jeffrey Fredberg & Ben Fabry

Abstract

Using a novel method that was both quantitative and reproducible, Francis Crick and Arthur Hughes (Crick and Hughes, 1950) were the first to measure the mechanical properties inside single, living cells. They concluded their groundbreaking work with the words:

> If we were compelled to suggest a model (of cell mechanics) we would propose Mother's Work Basket – a jumble of beads and buttons of all shapes and sizes, with pins and threads for good measure, all jostling about and held together by colloidal forces.

Thanks to advances in biochemistry and biophysics, we can now name and to a large degree characterize many of the beads and buttons, pins and threads. These are the scores of cytoskeletal proteins, motor proteins, and their regulatory molecules. But the traditional reductionist approach - to study one molecule at a time in isolation - has so far not led to a comprehensive understanding of how cells are able to perform such exceptionally complex mechanical feats as division, locomotion, contraction, spreading, or remodeling. The question then arises, even if all of the cytoskeletal and signaling molecules were known and fully characterized, would this information be sufficient to understand how the cell orchestrates complex and highly specific mechanical functions? Or put another way, do molecular events playing out at the nanometer scale necessarily add up in a straightforward manner to account for mechanical events at the micrometer scale?

We argue here that the answer to these questions may be 'No'. In the following chapter, we present a point of view that does not rely on a detailed knowledge of specific molecular functions and interactions, but instead focuses attention on dynamics of the microstructural arrangements between cytoskeletal proteins. Our thinking has been guided by recent advances in the physics of soft glassy materials. One of the more surprising findings that come out of this approach is the discovery that, independent of molecular details, a single, measurable quantity (called the 'noise temperature') seems to account for transitions between fluid-like and solid-like states of the cytoskeleton. Although the interpretation and precise meaning of this noise temperature is still emerging, it appears to give a measure of the 'jostling' and the 'colloidal forces' that act within the cytoskeleton.

1. Introduction

Measurements of mechanical properties afford a unique window into the dynamics of protein-protein interactions within the cell, with elastic energy storage reflecting numbers of molecular interactions, energy dissipation reflecting their rate of turnover, and remodeling events reflecting their spatio-temporal reorganization (Fredberg, Jones et al., 1996). As discussed in other chapters of this book, probes are now available that can measure each of these features with temporal resolution in the range of milliseconds, and spatial resolution in the range of nanometers. Using such probes, this chapter demonstrates that a variety of phenomena that have been taken as the signature of condensed systems in the glassy state are prominently expressed by the cytoskeletal lattice of the living adherent cell. While highly specific interactions play out on the molecular scale, and homogeneous behavior results on the integrative scale, evidence points to metastability of interactions and non-equilibrium cooperative transitions on the mesoscale as being central factors linking integrative cellular function to underlying molecular events. Insofar as such fundamental functions of the cell, including embryonic development, contraction, wound healing, crawling, metastasis, and invasion, all stem from underlying cytoskeletal dynamics, identification of those dynamics as being glassy would appear to set these functions into an interesting context.

The chapter begins with a brief summary of experimental findings in living cells. These findings are next described in terms of a remarkably simple empirical relationship that appears to capture the essence of the data with very few parameters. Finally, we show that this empirical relationship is predicted from the theory of soft glassy rheology (SGR). As such, SGR offers an intriguing perspective on mechanical behavior of the cytoskeleton and its relationship to the dynamics of protein-protein interactions.

2. Experimental findings in living cells

To study the rheology of cytoskeletal polymers requires a probe whose operative frequency range spans, insofar as possible, the internal molecular time scales of the rate processes in question. The expectation from such measurements is that the rheological behavior changes at characteristic relaxation frequencies, which in turn can be interpreted as the signature of underlying molecular interactions that dominate the response (Hill, 1965; Kawai and Brandt, 1980). Much of what follows in this chapter is an attempt to explain the failure to find such characteristic relaxation times in most cell types. The experimental findings of our laboratory, summarized below, are derived from single cell measurements using magnetic twisting cytometry (MTC) with optical detection of bead motion. Using this method, we were able to apply probing frequencies ranging from 0.01 Hz to 1 kHz. As shown by supporting evidence presented below, these findings are not peculiar to the method, rather they are consistent with those obtained using different methods such as atomic force microscopy (Alcaraz, Buscemi et al., 2003).

2.1 Magnetic Twisting Cytometry (MTC):

The MTC-device is a micro-rheometer in which the cell is sheared between a plate at the cell base (the cell culture dish upon which the cell is adherent) and a magnetic microsphere partially embedded into the cell surface as shown in Fig. 1. We use ferrimagnetic microbeads (4.5 μm diameter) that are coated with a panel of antibody and non-antibody ligands that allow them to bind to specific receptors on the cell surface (including various integrin subtypes, scavenger receptors, urokinase receptors, and immune receptors). The beads are magnetized horizontally by a brief and strong magnetic pulse, and then twisted vertically by an external homogeneous magnetic field that varies sinusoidally in time. This applied field creates a torque which causes the beads to rotate toward alignment with the field, like a compass needle aligning with the earth's magnetic field. This rotation is impeded, however, by mechanical forces that develop within the cell as the bead rotates. Lateral bead displacements during bead rotation in response to the resulting oscillatory torque are detected by a CCD camera mounted on an inverted microscope.

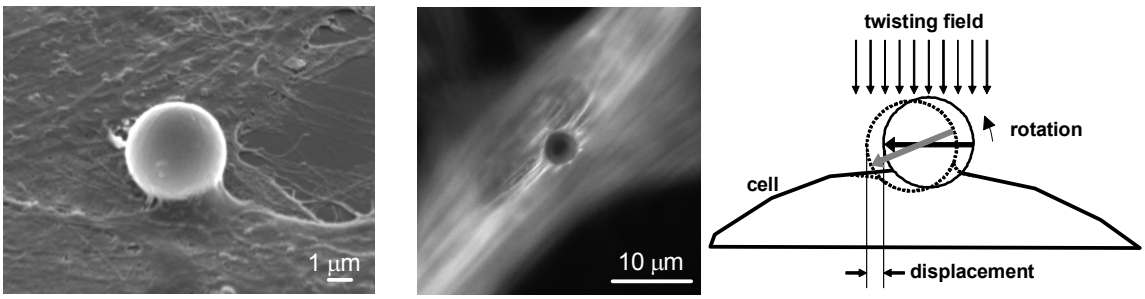

Fig. 1a (from (Fabry, Maksym et al., 2003)): Scanning EM of a bead bound to the surface of a human airway smooth muscle cell. 1b: Ferrimagnetic beads coated with an RGD-containing peptide bind avidly to the actin cytoskeleton (stained with fluorescently labeled phalloidin) of HASM cells via cell adhesion molecules (integrins). 1c: A magnetic twisting field introduces a torque which causes the bead to rotate and to displace. Large arrows indicate the direction of the bead's magnetic moment before (black) and after (gray) twisting. If the twisting field is varied sinusoidally in time, then the microbead wobbles to and fro, resulting in a lateral displacement, d, that can be measured.

Cell elasticity (g') and friction (g") can then be deduced from the magnitude and phase of the lateral bead displacements relative to the torque (Fig. 2). Image acquisition with short exposure times of 0.1 ms is phase-locked to the twisting field so that 16 images are acquired during each twisting cycle. Heterodyning (a stroboscopic technique) is used at twisting frequencies >1 Hz up to frequencies of 1000 Hz. The images are analyzed using an intensity-weighted center-of-mass algorithm in which sub-pixel arithmetic allows the determination of bead position with an accuracy of 5 nm (rms).

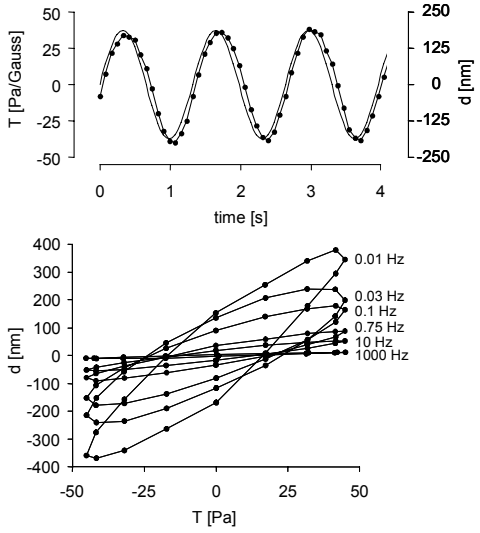

Fig. 2 (from (Fabry, Maksym et al., 2003)): a) Specific torque T (solid line) and lateral displacement d (filled circles connected by a solid line) vs. time in a representative bead measured at a twisting frequency of 0.75 Hz. Bead displacement followed the sinusoidal torque with a small phase lag. The filled circles indicate when the image and data acquisition was triggered, which was 16 times per twisting cycle. b) Loops of maximum lateral bead displacement vs. specific torque of a representative bead at different frequencies. With increasing frequency, displacement amplitude decreased.

2.2 Measurements of cell mechanics:

The mechanical torque of the bead is proportional to the external magnetic field (which was generated using an electromagnet), the bead's magnetic moment (which was calibrated by measuring the speed of bead rotation in a viscous medium), and the cosine between the bead's magnetization direction with the direction of the twisting field. Consider the specific torque of a bead, T, which is the mechanical torque per bead volume, and has dimensions of stress (Pa).

The ratio of the complex specific torque $\tilde{T}$ to the resulting complex bead displacement $\tilde{d}$ (evaluated at the twisting frequency) then defines a complex modulus of the cell $\tilde{g} = \tilde{T} / \tilde{d}$, and has dimensions of Pa/nm. These measurements can be transformed into traditional elastic shear (G') and loss (G") moduli by multiplication of g' and g" with a geometric factor that depends on the shape and thickness of the cell, and the degree of bead embedding. Finite element analysis of cell deformation for a representative bead-cell geometry (assuming homogeneous and isotropic elastic properties with 10% of the bead diameter embedded in a cell 5 μm high) sets this geometric factor to 6.8 μm (Mijailovich, Kojic et al., 2002). This geometric factor need serve only as a rough approximation, however, because it cancels out in the scaling procedure described below, which is model-independent. For each bead we compute the elastic modulus g' (the real part of $\tilde{g}$), the loss modulus g" (the imaginary part of $\tilde{g}$), and the loss tangent η (the ratio g"/g') at a given twisting frequency. These measurements are then repeated over a range of frequencies.

Since only synchronous bead movements that occur at the twisting frequency are considered, non-synchronous noise is suppressed by this analysis. Also suppressed are higher harmonics of the bead motion that may result from non-linear material properties and that – if not properly accounted for – could distort the frequency dependence of the measured responses. However, we found no evidence of non-linear cell behavior (such as strain-hardening or shear-thinning) at the level of stresses we apply with this technique, which ranges from about 1 Pa to about 130 Pa (Fig. 3). Throughout that range, which represents the physiological range, responses were linear.

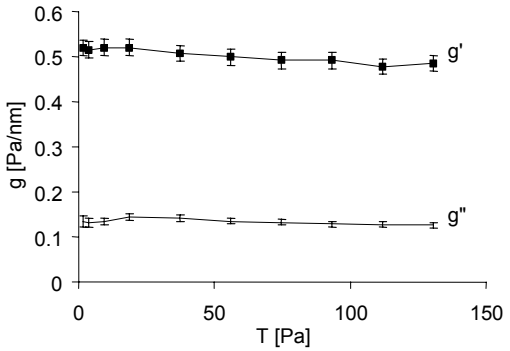

Fig. 3 (from (Fabry, Maksym et al., 2003)): g' and g" vs. specific torque amplitude T. g' and g" were measured in 537 HASM cells at f = 0.75 Hz. Specific torque amplitudes T varied from 1.8 to130 Pa. g' and g" were nearly constant, implying linear mechanical behavior of the cells in this range. Error bars indicate + one standard error.

2.3 Frequency dependence of g' and g":

The relationship of G' and G" vs. frequency for human airway smooth muscle (HASM) cells under control conditions is shown in Fig. 4, where each data point represents the median value of 256 cells. Throughout the frequency range studied G' increased with increasing frequency, f, according to a power law, f^{x-1} (as explained below, the formula is written in this way because the parameter x takes on a special meaning, namely, that of an effective temperature). Because the axes in Fig. 4 are logarithmic, a power law dependency appears as a straight line with slope x-1. The power law exponent of G' was 0.20 (x = 1.20), indicating only a weak dependency of G' on frequency. G" was smaller than G' at all frequencies except at 1 kHz. Like G', G" also followed a weak power law with nearly the same exponent at low frequencies. At frequencies larger than 10 Hz, however, G" exhibited a progressively stronger frequency dependence, approaching but never quite attaining a power law exponent of 1, which would be characteristic of a Newtonian viscosity.

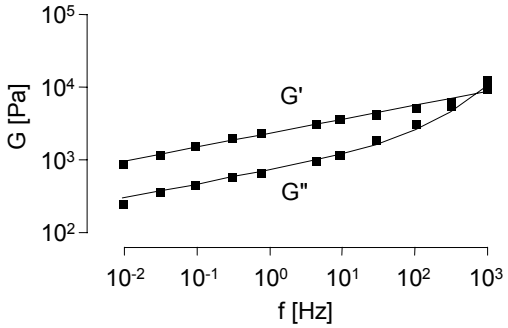

Fig. 4 (from (Fabry, Maksym et al., 2003)): G' and G" (median of 256 human airway smooth muscle cells) under control conditions measured at frequencies between 0.01 Hz and 1000 Hz. The solid lines were obtained by fitting Eq. 2 to the data. G' and G" (in units of Pa) were computed from the measured values of g' and g" (in units of Pa/nm) times a geometric factor α of 6.8 μm. G' increased with increasing frequency, f, according to a power law, f^{x-1}, with x = 1.20. G" was smaller than G' at all frequencies except at 1 kHz. At frequencies below 10 Hz, G" also followed a weak power law with nearly the same exponent as did G'; above 10 Hz the power law exponent increased and approached unity.

This behavior was at first disappointing because no characteristic time scale was evident; we were unable to identify a dominating relaxation process. The only characteristic time scale that falls out of the data is that associated with curvilinearity of the G" data that becomes apparent in the neighborhood of 100 Hz (Fig. 4). As shown below, this curvilinearity is attributable to a small additive Newtonian viscosity which is entirely uncoupled from cytoskeletal dynamics. This additive viscosity is on the order of 1 Pa s, or about 1000 fold higher than that of water and contributes to the energy dissipation (or friction) only above 100 Hz. Below 100 Hz, friction (G") remained a constant fraction (about 25%) of elasticity (G'). Such frictional behavior cannot be explained by a viscous dissipation process.

It is intriguing to note the combination of an elastic process (or processes) that increases with frequency according to a weak power-law over such a wide range of time scales, and a frictional modulus that, except at very high frequencies, is a constant, frequency-independent fraction of the elastic modulus. Similar behavior has been reported for a wide range of materials, biological tissue, and complex man-made structures such as airplane wings and bridges. Engineers use an empirical description – the structural damping equation (sometimes referred to as hysteretic damping law, or constant phase model) – to describe the mechanical behavior of such materials (Weber, 1841; Kohlrausch, 1866; Kimball and Lovell, 1927; Hildebrandt, 1969; Crandall, 1970; Fredberg and Stamenovic, 1989), but as regards mechanism, structural damping remains unexplained.

2.4 The structural damping equation:

The mechanical properties of such a material can be mathematically expressed either in the time domain or in the frequency domain. In the time domain, the mechanical stress response to a unit step change in strain imposed at t = 0 is an instantaneous component attributable to a pure viscous response together with a component that rises instantaneously and then decays over time as a power law,

$$g(t) = \mu\delta(t) + g_0(t/t_0)^{1-x} \qquad (1)$$

g_0 is the ratio of stress to the unit strain measured at an arbitrarily chosen time t_0, μ is a Newtonian viscous term, and $\delta(.)$ is the Dirac delta function. The stress-response to unit amplitude sinusoidal deformations can be obtained by taking the Fourier transform of the step response (Eq.1) and multiplying by $j\omega$, which gives the complex modulus $\tilde{g}(\omega)$ as

$$\tilde{g}(\omega) = g_0\left(\frac{\omega}{\Phi_0}\right)^{x-1}(1+i\bar{\eta})\ \Gamma(2-x)\ \cos\frac{\pi}{2}(x-1) + i\omega\mu \qquad (2)$$

where $\bar{\eta}$ = tan(x-1)π/2 and ω is the radian frequency 2πf (Hildebrandt, 1969). g_o and Φ_o are scale factors for stiffness and frequency respectively, Γ denotes the Gamma function, and i^2 is -1.

g_o and μ depend on bead-cell geometry. $\overline{\eta}$ has been called the structural damping coefficient (Fredberg and Stamenovic, 1989). The elastic modulus g' corresponds to the real part of Eq.2, which increases for all ω according to the power-law exponent, x-1. The loss modulus g" corresponds to the imaginary part of Eq.2 and includes a component which also increases as a power law with the same exponent. Therefore, the loss modulus is a frequency-independent fraction ($\overline{\eta}$) of the elastic modulus; such a direct coupling of the loss modulus to the elastic modulus is the characteristic feature of structural damping behavior (Fredberg and Stamenovic, 1989).

As mentioned already, the loss modulus includes a Newtonian viscous term, $j\omega\mu$, which turns out to be small except at very high frequencies. At low frequencies, the loss tangent η approximates $\overline{\eta}$. In the limit that x approaches unity, the power law slope approaches zero, g' approaches g_0 and $\overline{\eta}$ approaches zero. In the limit that x approaches 2, the power law slope approaches unity, g" approaches μ and $\overline{\eta}$ approaches infinity. Thus, Eq.2 describes a relationship between changes of the exponent of the power law and the transition from solid-like (x = 1, $\overline{\eta} = 0$) to fluid-like (x = 2, $\overline{\eta} = \infty$) behavior.

The structural damping equation describes the data in Fig. 4 exceedingly well and with only four free parameters: the scale factors g_o and Φ_o, the Newtonian viscosity μ, and the power-law exponent x-1. The structural damping coefficient $\overline{\eta}$ is not an independent parameter but depends on x only.

We now go on to show that three of the four parameters of the structural damping equation (g_o, Φ_o and μ) can be considered constant, and that changes in the cell's mechanical behavior during contraction, relaxation or other drug-induced challenges can be accounted for by changes of the parameter x alone.

2.5 Reduction of variables:

When smooth muscle cells are activated with a contractile agonist such as histamine, they generate tension, and their stiffness (G') increases, as has been shown in many studies (Warshaw, Rees et al., 1988; Fredberg, Jones et al., 1996; Hubmayr, Shore et al., 1996; Fabry, Maksym et al., 2001; Butler, Tolic-Norrelykke et al., 2002; Wang, Tolic-Norrelykke et al., 2002). Interestingly, in HASM cells this increase in G' after histamine activation (10^{-4} M) was more pronounced at lower frequencies. While G' still exhibited a weak power-law dependence on frequency, x fell slightly (Fig. 5). When cells were relaxed with DBcAMP (1 mM), the opposite happened: G' decreased, and x increased. When the actin cytoskeleton of the cells was disrupted with cytochalasin D (2 μM), G' decreased even more, while x increased further. Remarkably, the G' data defined a family of curves that, when extrapolated, appeared to intersect at a single value (G_0) at a very high frequency (Φ_0) (Fig. 5). Such a common intersection, or fixed point, of the G' vs. frequency curves at a very high frequency means that G_0 and Φ_0 were invariant with different drug treatments.

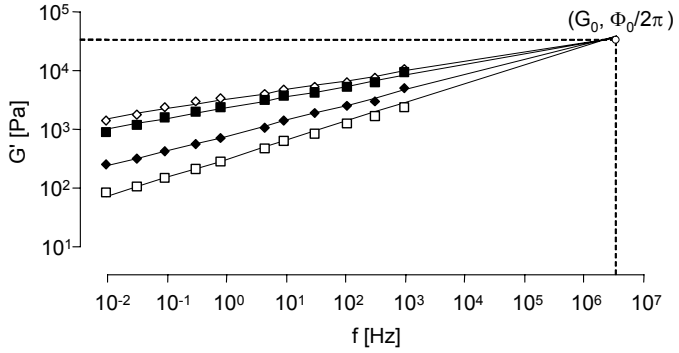

Fig. 5 (from (Fabry, Maksym et al., 2003)): G' vs. frequency in HASM cells under control conditions (■, n =256), and after 10 min treatment with the contractile agonist histamine [10^{-4} M] (◇, n =195), the relaxing agonist DBcAMP [10^{-3} M] (◆, n =239) and the actin-disrupting drug cytochalasin D [$2x10^{-6}$ M] (□, n =171). At all frequencies, treatment with histamine caused G' to increase, while treatment with DBcAMP and cytoD caused G' to decrease. Under all treatment conditions, G' increased with increasing frequency, f, according to a power law, f^{x-1}. x varied between 1.17 (histamine) and 1.33 (cytoD). A decreasing G' was accompanied by an increasing x, and vice versa. Solid lines are the fit of Eq.2 to the data. Surprisingly, these lines appeared to cross at a coordinate close to [G_0, $\Phi_0/2\pi$], well above the experimental frequency range. According to Eq.2, an approximate crossover implies that in the HASM cell the values of G_0 and Φ_0 were invariant with differing treatment conditions.

With all drug treatments, G' and G" tended to change in concert. The relationship between G" and frequency remained a weak power law at lower frequencies, and the power law exponent of G" changed in concert with that of G'. At the highest frequencies, the curves of G" vs. frequency for all treatments appeared to merge onto a single line with a power law exponent approaching unity (Fig. 6).

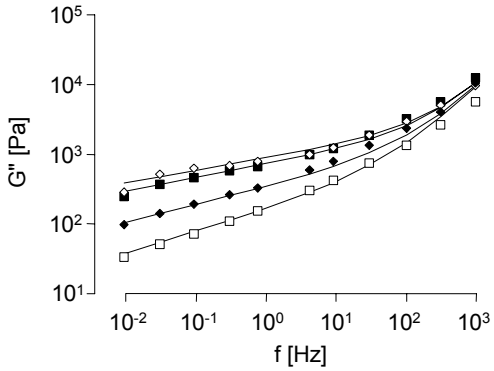

Fig. 6 (from (Fabry, Maksym et al., 2003)): G" vs. frequency in HASM cells under control conditions (■, n =256), and after 10 min treatment with histamine [10^{-4} M] (◇, n =195), DBcAMP [10^{-3} M] (◆, n =239) and cytochalasin D [$2x10^{-6}$ M] (□, n =171). At all frequencies, treatment with histamine caused G" to increase, while treatment with DBcAMP and cytoD caused G" to decrease. Under all treatment conditions, G" increased at frequencies below 10 Hz according to a power law, f^{x-1}, with exponents that were similar to that of the corresponding G'-data (Fig. 5). Above 10 Hz the power law exponents increased and approached unity for all treatments; the G" curves merged onto a single relationship.

The finding of a common intersection of the G' vs. f relationship stands up to rigorous statistical analysis, meaning that a 3-parameter fit of the structural damping equation (G_0, Φ_0 and x) to the full set G' data (measured over 5 frequency decades and with different pharmacological interventions) is not statistically different from a fit with G_0 and Φ_0 being fixed, and with x being the only free parameter (Fabry, Maksym et al., 2003). The very same set of parameters – a fixed value for G_0 and Φ_0 respectively, and a drug treatment dependent x – also predicts the G" vs. f relationship at frequencies below 100 Hz. Because the G" data appears to merge onto a single line at higher frequencies, a single Newtonian viscosity μ that is common for all drug treatments can account for the data, although a rigorous statistical analysis indicates that a negligible but significant improvement of the fit can be achieved with different μ-values for different drug treatments (Fabry, Maksym et al., 2003). For all practical purposes, therefore, the mechanical behavior of HASM cells is restricted to vary only in a very particular way such that a single parameter, x, is sufficient to characterize the changes of both cell elasticity and friction.

2.6 Universality:

This surprising and particular behavior is not restricted to HASM cells. We found the very same behavior – a power-law relationship of G' and G" vs. frequency, common intersection of the G' vs. f data for different drug treatments at a very high frequency, and merging of the G" vs. f data onto a single line – in all other animal and human cell types we have investigated so far, including macrophages, neutrophils, various endothelial and epithelial cell types, fibroblasts, and various cancer cell lines (Fabry, Maksym et al., 2001; Fabry, Maksym et al., 2003; Puig-de-Morales, Millet et al., 2004).

Power-law behavior and common intersection were also found with an almost exhaustive panel of drugs that target the actin cytoskeleton and the activity of myosin light chain kinase (including

BDM, ML-7, ML-9, W-7, various rho-kinase inhibitors, latrunculin, jasplakinolide) (Laudadio, Millet et al., 2005). Moreover, power-law behavior and common intersection are not peculiar to the details of the coupling between the bead and the cell, and can be observed in beads coated with different ligands (including RGD-peptide, collagen, vitronectin, fibronectin, urokinase, acetylated low-density lipoprotein) and antibodies that specifically bind to various receptors (activating and non-activating domains of various integrins and other cell adhesion molecules) (Puig-de-Morales, Millet et al., 2004). Neither is this behavior peculiar to the magnetic twisting technique. The power-law dependence of G' and G" on frequency is consistent with data reported for atrial myocytes, fibroblasts, and bronchial endothelial cells measured with atomic force microscopy (AFM), for pellets of mouse embryonic carcinoma cells measured with a disk rheometer, for airway smooth muscle cells measured with oscillatory magneto-cytometry, and for kidney epithelial cells measured by laser tracking of Brownian motion of intracellular granules (Shroff, Saner et al., 1995; Goldmann and Ezzell, 1996; Mahaffy, Shih et al., 2000; Maksym, Fabry et al., 2000; Yamada, Wirtz et al., 2000; Alcaraz, Buscemi et al., 2003). Using laser tracking microrheology, Yamada et al. also measured cell mechanics before and after microfilaments were disrupted with Latrunculin A, and obtained two curves of G' vs. f that intersected at a frequency comparable to the value we measured with our magnetic twisting technique, as shown in Figure 7 (Yamada, Wirtz et al., 2000).

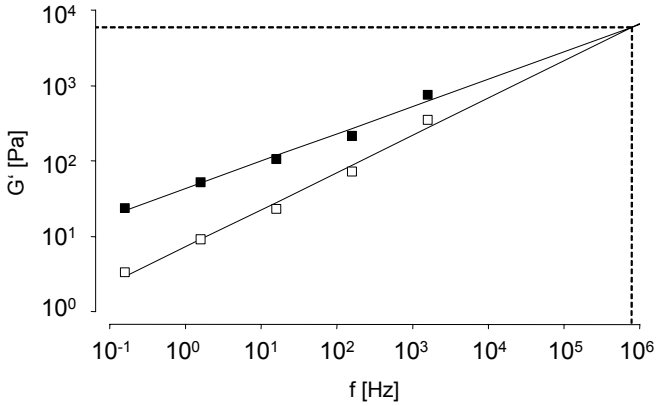

Fig. 7 (adapted from (Yamada, Wirtz et al., 2000)). G' vs. frequency in kidney epithelial cells measured with laser tracking microrheology under control conditions (■), and after 15 min treatment with Latrunculin A [$1x10^{-6}$ M] (□). Solid lines are the fit of Eq.2 to the data, with x = 1.36 under control conditions, and x = 1.5 after Latrunculin A treatment. These lines crossed at G_0 = 5.48 kPa and $\Phi_0 = 6.64*10^5$ Hz.

Finally, power-law behavior in the frequency domain (Eq. 2) corresponds to power-law behavior in the time domain (Eq. 1): when we measured the creep modulus of the cells by applying a step change of the twisting field, we did indeed find power-law behavior of the creep modulus vs. time, and a common intersection of the data at a very short time (Lenormand, Millet et al., 2004).

2.7 Scaling the data:

Not surprisingly, although structural damping behavior always prevailed, substantial differences were observed in the absolute values of our G' and G" measurements between different cell lines, and even larger (up to two orders of magnitude) differences when different bead coatings were used (Fabry, Maksym et al., 2001; Puig-de-Morales, Millet et al., 2004). Still larger (up to three orders of magnitude) differences were observed between individual cells of the same type even when they were grown within the same cell well (Fabry, Maksym et al., 2001). It is difficult to specify to what extent such differences reflect true differences in the "material" properties between different cells or between different cellular structures to which the beads are attached, versus differences in the geometry (cell height, contact area between cell and bead, etc.). Theoretically, these geometric details could be measured and then modeled, but in practice such measurements and models are inevitably quite rough (Mijailovich, Kojic et al., 2002).

Rather than analyzing "absolute" cell mechanics, it is far more practical (and insightful as shown below) to focus attention instead upon relative changes in cell mechanics. To first order,

such relative changes are independent of bead-cell geometry. Thus, the measurements need to be normalized or scaled appropriately such that each cell serves as its own control.

Two such scaled parameters have already been introduced: The first one is the slope of the power-law relationship (x-1), which is the log change in G' or G" per frequency decade (e.g. the ratio of G'_{10Hz}/G'_{1Hz}). The second scaled parameter is the hysteresivity η, which is the ratio between G" and G' at a single frequency.

Both scaling procedures cause factors (such as bead-cell geometry) that equally affect the numerator and denominator of those ratios to cancel out. Moreover, both scaling procedures can be performed on a bead-by-bead basis. The bead-by-bead variability of both x and η are negligible when compared with the huge variability in G' (Fabry, Maksym et al., 2001; Fabry, Maksym et al., 2001).

A third scaling parameter is the normalized stiffness G_n, which we define as the ratio between G' (measured at a given frequency, say 0.75 Hz) and G_0 (the intersection of the G' vs. f curves from different drug treatments, Fig. 5). Here, G_0 serves as an internal stiffness scale that is characteristic for each cell type and for each bead coating (receptor-ligand interaction), but that is unaffected by drug treatments. Thus, the normalized stiffness G_n allows us to compare the drug-induced responses of cells under vastly different settings, such as different bead coating etc.

2.8 Collapse onto master curves:

The data were normalized as follows. We estimated x from the fit of Eq.2 to the pooled (median over many cells) g' and g" data. The hysteresivity η was estimated from ratio of g"/g' measured at 0.75 Hz (an arbitrary choice). The normalized cell stiffness G_n was estimated as g' measured at 0.75 Hz divided by g_0. log G_n vs. x and η vs. x graphs were then plotted (Fig.8).

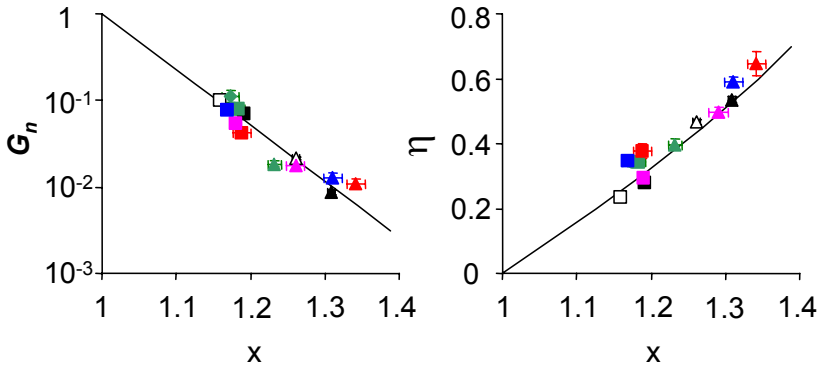

Fig.8 (from (Fabry, Maksym et al., 2003)): Normalized stiffness G_n vs. x (left) and hysteresivity η (right) vs. x, of HASM cells (black, n = 256), human bronchial epithelial cells (blue, n = 142), mouse embryonic carcinoma cells (F9) cells (pink, n = 50), mouse macrophages (J774A.1) (red, n = 46) and human neutrophils (green, n = 42) under control conditions (■), treatment with histamine (□), FMLP (◆), DBcAMP (Δ) and cytochalasin D (▲). x was obtained from the fit of Eq.2 to the pooled (median) data. Drugs that increased x caused the normalized stiffness G_n to decrease and hysteresivity η to increase, and vice versa. The normalized data for all types collapsed onto the same relationships. The structural damping equation by (Eq. 2) is depicted by the black solid curves: $\ln G_n = (x-1)\ln(\omega/\Phi_0)$ with $\Phi_0 = 2.14 \times 10^7$ rad/s, and $\overline{\eta} = \tan((x-1)\pi/2)$. Error bars indicate $\pm$ one standard error. If x is taken to be the noise temperature, then these data suggest that the living cell exists close to a glass transition and modulates its mechanical properties by moving between glassy states that are "hot", melted and liquidlike, and states that are "cold", frozen and solidlike. In the limit that x approaches 1 the system behaves as an ideal Hookean elastic solid, and in the limit that x approaches 2 the system behaves as an ideal Newtonian fluid (Eq. 2).

In human airway smooth muscle (HASM) cells, we found that drugs that increased x caused the normalized stiffness G_n to decrease (Fig. 8a, black symbols). The relationship between log G_n and x appears as nearly linear: $\ln G_n \sim -x$. The solid line in Fig. 8a is the prediction from the structural damping equation under the condition of a common intersection of all G' data at radian frequency Φ_0:

$$\ln G_n = (x-1) \ln (\omega/\Phi_0). \qquad (3)$$

How close the normalized data fell to this prediction thus indicates how well a common intersection can account for those data.

Conversely, drugs that increased x caused the normalized frictional parameter η to increase (Fig. 8b, black symbols). The solid line in Fig. 8b is the prediction from (and not a fit of) the structural damping equation:

$$\eta = \tan(x-1)\pi/2. \quad (4)$$

How close the normalized data fell to this prediction thus indicates how well the structural damping equation can account for those data.

Surprisingly, the normalized data for the other cell types collapsed onto the very same relationships that were found for HASM cells (Fig. 8). In all cases, drugs that increased x caused the normalized stiffness G_n to decrease and hysteresivity η to increase. These relationships thus represent universal master curves in that a single parameter, x, defined the constitutive elastic and frictional behaviors for a variety of cytoskeletal manipulations, for 5 frequency decades, and for diverse cell types.

The normalized data from all cell types and drug treatments fell close to the predictions of the structural damping equation (Fig. 8). In the case of the η vs. x data (Fig. 8b), this collapse of the data indicates that the coupling between elasticity and friction, and their power-law frequency dependence, is well described by the structural damping equation. In the case of the log G_n vs. x data (Fig. 8a), the collapse of the data indicates a common intersection of the G vs. f curves exists for all cell types, and that this intersection occurs approximately at the same frequency Φ_0.

Rigorous statistical analysis of the data from many different cell types has thus far supported the existence of a common intersection of the G' vs. f relationships measured after treatment with a large panel of cytoskeletally active drugs (Laudadio, Millet et al., 2005). This holds true regardless of the receptor-ligand pathway that was used to probe cell rheology (Puig-de-Morales, Millet et al., 2004). The same statistical analysis, however, hints that the crossover frequency Φ_0 may not be the same for all cell types and receptor-ligand pathways. Unfortunately, so far Φ_0 cannot be measured with high enough accuracy to resolve such differences. Thus for all practical purposes we can regard Φ_0 as being the same for all cell types and for all receptor-ligand combinations (Fabry, Maksym et al., 2003; Puig-de-Morales, Millet et al., 2004).

The structural damping relationship has long been applied to describe the rheological data for a variety of biological tissues (Weber, 1835; Kohlrausch, 1847; Fung, 1967; Hildebrandt, 1969; Fredberg and Stamenovic, 1989; Suki, Peslin et al., 1989; Hantos, Daroczy et al., 1990; Navajas, Mijailovich et al., 1992; Fredberg, Bunk et al., 1993). Thus, it may seem natural (but still intriguing) that living cells too exhibit structural damping behavior, and in this regard the collapse of the η vs. x data from different cell types and drug treatments onto the same relationship (Fig.8b) is a necessary consequence of such behavior. But it is utterly mystifying why the G_n vs. x data from different drug treatments should form any relationship at all, and why, moreover, the data from different cell types and different receptor-ligand pathways should collapse onto the very same relationship.

3. Theory of soft glassy rheology

3. 1 What are soft glassy materials:

The master relationships shown in Figs. 8 and 9 demonstrate that when the mechanical properties of the cell change, they do so along a special trajectory. This trajectory is found to be identical in a large variety of cell types that are probed via different receptor-ligand pathways and over many frequency decades. In all those cases, changes of stiffness and friction induced by pharmacological interventions could be accounted for solely by changes in x. This parameter x appears to play a central organizing role leading to the collapse of all data onto master curves. But what is x?

A possible answer to the above question may come – surprisingly – from a theory of soft glassy materials that was developed by Sollich and colleagues (Sollich, Lequeux et al., 1997). In the remainder of this chapter a brief introduction is given into some fundamental principles and ideas about soft glassy rheology; parallels between living cells and soft glassy materials are shown, and a discuss ion ensues on what insights may be gained from this into the mechanisms involved.

The class of soft glassy materials (SGM) comprises what would at first glance seem to be a remarkably diverse group of substances that includes foams, pastes, colloids, emulsions and slurries. Yet, the mechanical behavior of each of these substances is surprisingly alike. The common empirical criteria that define this class of materials are that they are very soft (in the range of Pa to kPa), that both G' and G" increase with the same weak power law dependencies on frequency, and that the loss tangent η is frequency insensitive and of the order 0.1 (Sollich, Lequeux et al., 1997; Sollich, 1998). The data presented above establish that the cytoskeleton of living cells satisfies all of these criteria. Accordingly, we propose the working hypothesis that the cytoskeleton of the living cell can be added to the list of soft glassy material.

Sollich reasoned that because the materials comprising this class are so diverse, the common rheological features must be not so much a reflection of specific molecules or molecular mechanisms as they are a reflection of generic system properties that play out at some higher level of structural organization (Sollich, 1998). The generic features that all soft glassy materials share are that each is composed of elements that are discrete, numerous and aggregated with one another via weak interactions. In addition, these materials exist far away from thermodynamic equilibrium and are arrayed in a microstructural geometry that is inherently disordered and metastable. Note that the cytoskeleton of living cells shares all of these features.

3.2 Sollich's theory of SGMs:

To describe the interaction between the elements within the matrix, Sollich developed a theory of soft glassy rheology (SGR) using earlier work by Bouchaud as a point of departure (Bouchaud, 1992). SGR theory considers that each individual element of the matrix exists within an energy landscape containing many wells, or traps, of differing depth E. These traps are formed by interactions of the element with neighboring elements. In the case of living cells those traps might be plausibly thought to be formed by binding energies between neighboring cytoskeletal elements including but not limited to cross-links between actin filaments, cross-bridges between actin and myosin, hydrophilic interactions between various proteins, charge effects or simple steric constraints.

In Bouchaud's theory of glasses, an element can escape its energy well and fall into another nearby well; such hopping events are activated by thermally driven random fluctuations. As distinct from Bouchaud's theory, in Sollich's theory of soft glassy materials each energy well is regarded as being so deep that the elements are unlikely to escape the well by thermal fluctuations alone. Instead, elements are imagined to be agitated, or jostled, by their mutual interactions with neighboring elements (Sollich 1998). A clear notion of the source of the non-thermal agitation remains to be identified, but this agitation can be represented nonetheless by an effective temperature, or noise level, x.

Sollich's SGR theory follows from a conservation law for probability of an element being trapped in an energy well of depth *E* and local displacement (strain) *l*, at time *t*, denoted $P(E,l,t)$. Dynamics is then governed by a conservation equation for this probability, given by

$$\partial \mathrm{P}(\mathrm{E},\mathrm{l},\mathrm{t})/\partial \mathrm{t} + \gamma \partial \mathrm{P}/\partial \mathrm{l} = -\mathrm{g}(\mathrm{E},\mathrm{l})\mathrm{P}(\mathrm{E},\mathrm{l},\mathrm{t}) + \mathrm{f}(\mathrm{E})\Phi(\mathrm{t})\delta(\mathrm{l}) \qquad (5)$$

where $\Phi(t) = \int dEdl\ g(E,l)P(E,l,t)$ (required for conservation of probability), and $\delta(\cdot)$ is the Dirac delta function. Here $\gamma = dl/dt$ and *f(E)* is the distribution of energy well depths. Eq. 5 states that the material rate of change of *P* is given by the sum of two terms. The first term is depletion, equal to the probability of resident elements hopping out, given by the product of the probability of occupancy *P* and a transition rate $g(E,l)$. The second term is the accumulation

rate, equal to the product of the total number of available transitions $\Phi(t)$ and the delta function constraint forcing elements to hop into wells at zero local strain.

Sollich takes $g(E,l) = \Phi_0 \exp(-(E + kl^2/2)/x)$ and f(E) = Φ_0 exp (-*E*), respectively. Note that the transition rate $g(E,l)$ for hopping out of wells is distributed over *E*, and which, in the nonlinear regime, is also a function of strain. Note further that the transition rate into wells of depth *E* only depends on strain through the constraint that $l = 0$ following a hop.

When x > 1, there is sufficient agitation in the matrix that the element can hop randomly between wells and, as a result, the system as a whole can flow and become disordered. When x approaches 1, however, the elements become trapped in deeper and deeper wells from which they are unable to escape - the system exhibits a glass transition and becomes a simple elastic solid with stiffness G_0.

3.3 Soft glassy rheology and structural damping:

Remarkably, in the limit that the frequency is small (compared to Φ_0) and the imposed deformations are small (such that the rate for hopping out of wells is dominated by x), Sollich's theory leads directly to the structural damping equation (Eq. 2).

The data reported above establish firmly that the mechanical behavior of cells conform well to Eq. 2. If Sollich's theory and underlying ideas are assumed to apply to the data reported here, then the parameters in Eq.2 (x, G_0, Φ_0) can be identified as follows.

The parameter x is identified as being the noise temperature of the cytoskeletal matrix. The measured values of x in cells lie between 1.15 and 1.35, indicating that cells exist close to a glass transition.

G_0 is identified as being the stiffness of the cytoskeleton at the glass transition (x=1). In this connection, Satcher and Dewey (Satcher and Dewey, 1996) developed a static model of cell stiffness based on consideration of cell actin content and matrix geometry. All dynamic interactions were neglected in their model, as would be the case in SGR theory in the limit that x approaches 1, when all hopping ceases. As such, it might be expected that their model would predict this limiting value of the stiffness, G_0, as defined in Eq. 2. Indeed, we have found a remarkably good correspondence between their prediction (order of 10 kPa) and our estimate for G_0 (41 kPa in HASM cells).

Finally, Φ_0 is identified in Sollich's theory as being the maximum rate at which cytoskeletal elements can escape their traps. However, for soft glassy materials in general, and the case of living cells in particular, the factors that determine Φ_0 remain unclear. Statistical analysis of our data suggests that Φ_0 did not vary with drug treatments and possibly not even across cell type (Fig. 7). But why Φ_0 is invariant is not at all clear, and is not explained by SGR theory.

3.4 Open questions

Crucial aspects of soft glassy rheology (SGR) theory remain incomplete, however. First, the effective noise temperature x is a temperature to the extent that the rate at which elements can hop out of a trap assumes the form exp(-E/x), where x takes the usual position of a thermal energy kT in the familiar Boltzmann exponential. By analogy, x has been interpreted by Sollich as reflecting jostling of elements by an unidentified but non-thermal origin. It appears an interesting question whether the ambiguity surrounding x might be resolved in the case of living cells (as opposed to the inert materials for which SGR theory was originally devised) by an obvious and ready source of non-thermal energy injection, namely, those proteins that go through cyclic conformational changes and thus agitate the matrix by mechanisms that are ATP-dependent.

Second, Sollich interprets *E* as an energy well depth, but there are difficulties with this interpretation. In SGR theory the total energy is not a conserved quantity even in the zero strain case, and the energy landscape has no spatial dimension, precluding explicit computation of

microstructural rearrangements. Such microstructural rearrangements in the form of cytoskeletal reorganization during cell division, crawling or intracellular transport processes are of fundamental interest in cell biology. The fluctuation-dissipation theorem implies a profound connection between dissipative phenomena as reflected in the measured values of G" during oscillatory forcing, and the temporal evolution of the mean square displacement (MSD), or fluctuations, of free unforced particles in the medium. Experiments from our lab and others revealed a behavior of MSD that lies somewhere between that of simple diffusion in a homogeneous medium, and ballistic behavior characteristic of short time displacements (An, Fabry et al., 2004). To what extent this is consistent with SGR theory also remains an open question (Lau, Hoffman et al., 2003).

Despite these questions, however, it is clear from Sollich's theory that for a soft glass to elastically deform, its elements must remain in energy wells; in order to flow, the elements must hop out of these wells. In the case of cells, these processes depend mainly on a putative energy level in the cytoskeletal lattice, where that energy is representative of the amount of molecular agitation, or jostling, present in the lattice relative to the depth of energy wells that constrain molecular motions. This energy level can be expressed as an effective lattice temperature (x) – as distinct from the familiar thermodynamic temperature. Even while the thermodynamic temperature is held fixed, this effective temperature can change, can be manipulated, and can be measured. The higher the effective temperature, the more frequently do elemental structures trapped in one energy well manage to hop out of that well only to fall into another. The hop, therefore, can be thought of as the fundamental molecular remodeling event.

It is interesting that, from a mechanistic point of view, the parameter x plays a central role in the theory of soft glassy materials. At the same time, from a purely empirical point of view, the parameter x is found to play a central organizing role leading to the collapse of all data onto master curves (Fig. 8). Whether or not the measured value of x might ultimately be shown to correspond to an effective lattice temperature, this empirical analysis would appear to provide a unifying framework for studying protein interactions within the complex integrative microenvironment of the cell body.

In the next section, the concepts developed above are employed to tie together within such a unified framework diverse behavior of cell physiology that were previously unexplained or regarded as unrelated.

4. Biological insights from SGR theory

4.1 Malleability of airway smooth muscle:

The function of smooth muscle is to maintain shape and/or tone of hollow organs (Murphy, 1988). Typically, smooth muscle must do so over an extremely wide range of working lengths. Two unique features enable smooth muscle to do this. First, smooth muscle can develop its contractile forces almost independently of muscle length (Wang, Pare et al., 2001). To achieve this, the cytoskeletal lattice and associated contractile machinery of smooth muscle is disordered and highly malleable, quite unlike the ordered and fixed structure of striated muscle and the rather narrow range of lengths over which striated muscle can generate appreciable tension. Second, at the height of force development, smooth muscle can "latch" its contractile machinery, that is to say, down-regulate the rate of acto-myosin cycling, thereby leading to tone maintenance very economically in terms of energy metabolism (Hai and Murphy, 1989). To produce the same steady state isometric force, for example, striated muscle hydrolyzes more ATP at a rate 300 times higher than does smooth muscle (Murphy, 1988).

Soft glass rheology (SGR) theory helps to piece together such information into an integrative context. Below, we present some earlier data from our laboratory on the mechanical and contractile properties of smooth muscle tissue; these data contained some previously unexplained loose ends. The glass hypothesis now offers a new and consistent explanation of these data.

Our earlier work focused on the contractile states of smooth muscle that were inferred from the responses to sinusoidal length or force perturbations. Fig. 9 summarizes a typical result obtained from sinusoidal length perturbations..

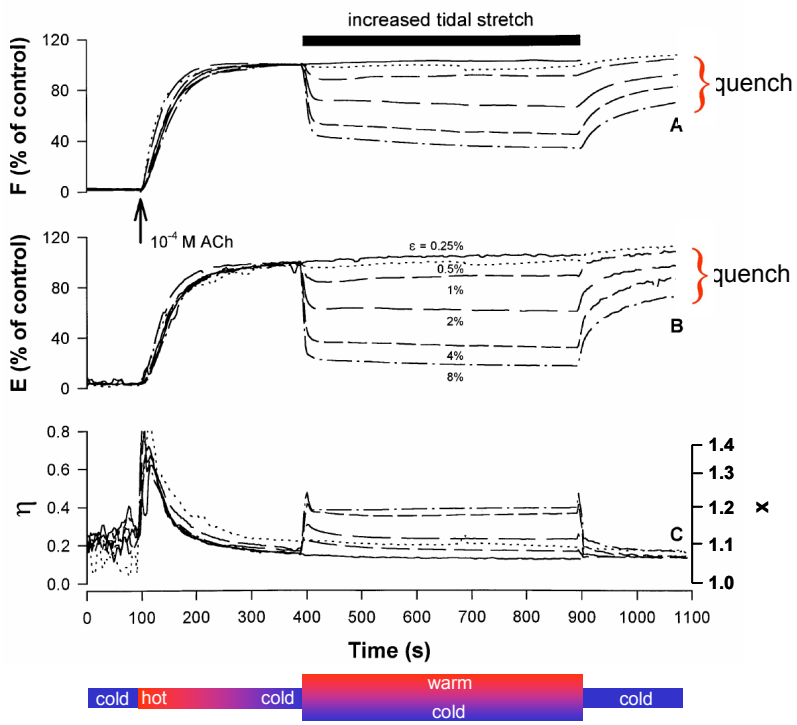

Fig. 9 (adapted from (Fredberg, Inouye et al., 1997)): Time courses of force (A), stiffness (B), and hysteresivity (C) in a bovine tracheal smooth muscle strip. To continuously track changes in stiffness and hysteresivity, sinusoidal length oscillations at a frequency of 0.2 Hz and with amplitude ε were superimposed throughout the measurement period. The tangent of the phase angle between the sinusoidal length oscillations and the resulting force oscillations (i.e., the hysteresivity η) defines the noise temperature x (panel C right side) by a simple relationship (Equ. 5). The strip was stimulated at 100 s with acetylcholine (10^{-4} M). The solid trace in each panel corresponds to ε maintained throughout at 0.25%. Broken lines correspond to runs in the same muscle subjected to graded increments of ε from 0.25 to either 0.5, 1, 2, 4,or 8% over the time interval from 400 to 900 s.

The stiffness E in those experiments is a measure of the number of force-generating acto-myosin bridges, while the hysteresivity η is a measure of internal mechanical friction and is closely coupled to the rate of crossbridge cycling as reflected both in the unloaded shortening velocity and the rate of ATP utilization measured by NADH fluorimetry (Fredberg, Jones et al., 1996). The dramatic increase in force and stiffness after contractile stimulation (Fig. 9) therefore reflects an increase in the number of acto-myosin bridges. The progressive fall of η after contractile stimulus onset (Fig. 9) has been interpreted as reflecting rapidly cycling crossbridges early in the contractile event converting to slowly cycling latch bridges later in the contractile event (Fredberg, Jones et al., 1996). This molecular picture fits exceptionally well with computational analysis based on first principles of myosin binding dynamics. According to this picture, imposed sinusoidal length oscillations (between 400 s and 900 s in Fig. 9) around a constant mean length lead to a disruption of acto-myosin cross-bridges and latch-bridges. This shifts the binding equilibrium of myosin towards a faster cycling rate such that with increasing oscillation amplitude hysteresivity increases, and muscle force and stiffness fall (Fredberg, 2000; Mijailovich, Butler et al., 2000). However, this picture is unable to explain why force and stiffness remained suppressed even after the length oscillations had stopped (Fig. 9).

Much the same behavior was found in a similar experiment in which force oscillations were imposed around a constant mean force (Fredberg, 2000): With increasing amplitude of the force

oscillations, stiffness decreased, and muscle length and hysteresivity increased (Fig. 10). Again, this behavior was exceptionally well explained by acto-myosin binding dynamics (Fredberg, 2000), but when the amplitude of the force oscillations was reduced, length and stiffness inexplicably did not return (Fig. 10).

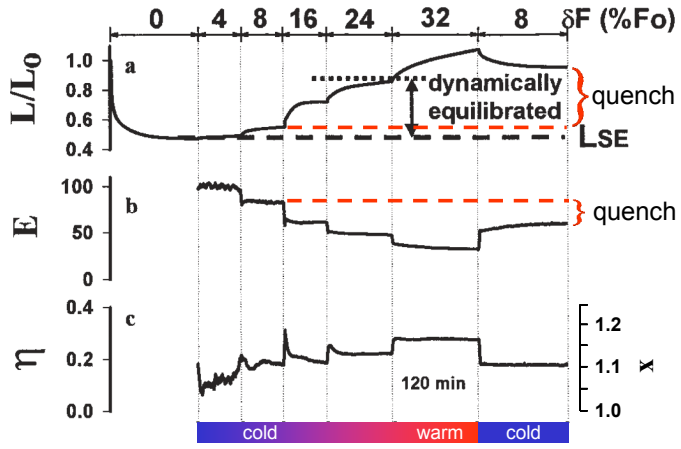

Fig. 10 (adapted from (Fredberg, 2000)): Evolution of mechanical properties of bovine tracheal smooth muscle during contraction against a constant mean force on which force fluctuations (0.2 Hz) of graded amplitude δF were superimposed. (a) Mean muscle length (relative to optimal length L_0). (b) Loop stiffness (percentage of maximum isometric value). (c) hysteresivity η and noise temperature x. L_{SE} is the statically equilibrated length of the muscle after 120 min of unperturbed contraction against a constant load of 32% of maximum force (F_0).

A rather different perspective on these observations (Fig. 9 and10) arises when they are viewed instead through the lens of glassy behavior. Accordingly, the relaxed smooth muscle cell is in a relatively "cold" state, with a noise temperature close to unity, but with the onset of contractile stimulation the cell very rapidly becomes “hot”. After this hot initial transient, the cell then begins to gradually “cool” in the process of sustained contractile stimulation, until, eventually, it approaches a steady state that approximates a “frozen” state not only mechanically (high stiffness and low noise temperature) but also biochemically and metabolically (Gunst and Fredberg, 2003).

The progressive decrease of stiffness and increase of hysteresivity with increasing amplitude of the imposed cyclic strain (Fig. 9 and 10) is consistent with a fluidization of the CSK matrix due to the application of a shear stress. SGR theory predicts that shear stress imposed at the macroscale adds to the agitation already present at the microscale, and thereby increases the noise temperature in the matrix (Sollich, 1998). This in turn allows elements to escape their cages more easily such that friction and hysteresivity increases, while stiffness decreases (Sollich, 1998; Fabry and Fredberg, 2003).

SGR theory now goes beyond the theory of perturbed myosin binding by predicting that the stretch-induced increase in noise temperature speeds up all internal molecular events, including accelerated plastic restructuring events within the CSK. When the tidal stretches are terminated (Fig. 9 and 10), however, the noise temperature is suddenly lowered, and all plastic changes might become trapped, or quenched, so that the muscle is unable to return to maximum force and stiffness (Fig. 9), or maximum shortening (Fig. 10) (Fabry and Fredberg, 2003).

The glass hypothesis predicts, therefore, that the cell ought to be able to adapt faster to step length changes imposed while the cell is transiently ‘hot’ (i.e. early in activation), and far less so after it has cooled in the process of sustained activation (Fabry and Fredberg, 2003; Gunst and Fredberg, 2003). Indeed, Gunst and colleagues showed that a step change of muscle length alters the level of the subsequent force plateau to a degree that depends mostly on the timing of the length change with respect to stimulus onset (Gunst, Meiss et al., 1995; Gunst and Fredberg, 2003).

5. Concluding remarks

The behavior of soft glasses, and the underlying notion of the noise temperature, might provide a unifying explanation of the ability of the cytoskeletal lattice to deform, to flow and to remodel. Such a view does not point to specific molecular processes that occur, but instead derives the mechanical properties from generic features: structural elements that are discrete, numerous, aggregated with one another via weak interactions, and arrayed in a geometry that is structurally disordered and metastable. We have proposed here that these features may comprise the basis of CSK rheology and remodeling.

References

Alcaraz, J., L. Buscemi, et al. (2003). Microrheology of human lung epithelial cells measured by atomic force microscopy. ***Biophys J***, 84, 2071-9.

An, S. S., B. Fabry, et al. (2004). Role of Heat Shock Protein 27 in Cytoskeletal Remodeling of the Airway Smooth Muscle Cell. ***J Appl Physiol***, 96, 1701-1713.

Bouchaud, J. (1992). Weak ergodicity breaking and aging in disordered systems. ***J Phys I***, 2, 1705-1713.

Butler, J. P., I. M. Tolic-Norrelykke, et al. (2002). Traction fields, moments, and strain energy that cells exert on their surroundings. ***Am J Physiol Cell Physiol***, 282, C595-605.

Crandall, S. H. (1970). The role of damping in vibration theory. ***J Sound Vibr***, 11, 3-18.

Crick, F. H. C. and A. F. W. Hughes (1950). The physical properties of cytoplasm. ***Exp Cell Res***, 1, 37-80.

Fabry, B. and J. J. Fredberg (2003). Remodeling of the airway smooth muscle cell: are we built of glass? ***Respir Physiol Neurobiol***, 137, 109-24.

Fabry, B., G. N. Maksym, et al. (2001). Scaling the microrheology of living cells. ***Phys Rev Lett***, 87, 148102.

Fabry, B., G. N. Maksym, et al. (2003). Time scale and other invariants of integrative mechanical behavior in living cells. ***Phys. Rev. E***, 68, 041914.

Fabry, B., G. N. Maksym, et al. (2001). Time course and heterogeneity of contractile responses in cultured human airway smooth muscle cells. ***J Appl Physiol***, 91, 986-94.

Fredberg, J. J. (2000). Airway smooth muscle in asthma. Perturbed equilibria of myosin binding. ***Am J Respir Crit Care Med***, 161, S158-60.

Fredberg, J. J., D. Bunk, et al. (1993). Tissue resistance and the contractile state of lung parenchyma. ***J Appl Physiol***, 74, 1387-97.

Fredberg, J. J., D. Inouye, et al. (1997). Airway smooth muscle, tidal stretches, and dynamically determined contractile states. ***Am J Respir Crit Care Med***, 156, 1752-9.

Fredberg, J. J., K. A. Jones, et al. (1996). Friction in airway smooth muscle: mechanism, latch, and implications in asthma. ***J Appl Physiol***, 81, 2703-12.

Fredberg, J. J. and D. Stamenovic (1989). On the imperfect elasticity of lung tissue. ***J Appl Physiol***, 67, 2408-19.

Fung, Y. C. (1967). Elasticity of soft tissues in simple elongation. ***Am J Physiol***, 213, 1532-44.

Goldmann, W. H. and R. M. Ezzell (1996). Viscoelasticity in wild-type and vinculin-deficient (5.51) mouse F9 embryonic carcinoma cells examined by atomic force microscopy and rheology. ***Exp Cell Res***, 226, 234-7.

Gunst, S. J. and J. J. Fredberg (2003). The first three minutes: smooth muscle contraction, cytoskeletal events, and soft glasses. ***J Appl Physiol***, 95, 413-25.

Gunst, S. J., R. A. Meiss, et al. (1995). Mechanisms for the mechanical plasticity of tracheal smooth muscle. ***Am J Physiol***, 268, C1267-76.

Hai, C. M. and R. A. Murphy (1989). Cross-bridge dephosphorylation and relaxation of vascular smooth muscle. ***Am J Physiol***, 256, C282-7.

Hantos, Z., B. Daroczy, et al. (1990). Modeling of low-frequency pulmonary impedance in dogs. ***J Appl Physiol***, 68, 849-60.

Hildebrandt, J. (1969). Comparison of mathematical models for cat lung and viscoelastic balloon derived by Laplace transform methods from pressure-volume data. ***Bull Math Biophys***, 31, 651-67.

Hill, A. V. (1965). ***Trails and Trials in Physiology (pp. 14-15)***. London, E. Arnold.

Hubmayr, R. D., S. A. Shore, et al. (1996). Pharmacological activation changes stiffness of cultured human airway smooth muscle cells. ***Am J Physiol***, 271, C1660-8.

Kawai, M. and P. W. Brandt (1980). Sinusoidal analysis: a high resolution method for correlating biochemical reactions with physiological processes in activated skeletal muscles of rabbit, frog and crayfish. ***J Muscle Res Cell Motil***, 1, 279-303.

Kimball, A. L. and D. E. Lovell (1927). Internal Friction in Solids. ***Phys Rev***, 30, 948–959.

Kohlrausch, F. (1866). Beiträge zur Kenntniss der elastischen Nachwirkung. ***Ann Phys Chem***, 128, 1-20, 207-227, 399-419.

Kohlrausch, R. (1847). Nachtrag ueber die elastische Nachwirkung beim Cocon- und Glasfaden, und die hygroskopische Eigenschaft des ersteren. ***Ann Phys Chem***, 72, 393-398.

Lau, A. W., B. D. Hoffman, et al. (2003). Microrheology, stress fluctuations, and active behavior of living cells. ***Phys Rev Lett***, 91, 198101.

Laudadio, R. E., E. J. Millet, et al. (2005). Rheology of the rat airway smooth muscle cell: scaling of responses to actin modulation. ***Am J Physiol***, in review.

Lenormand, G., E. Millet, et al. (2004). Linearity and time-scale invariance of the creep function in living cells. ***J Royal Soc Interface***, 1, 91-97.

Mahaffy, R. E., C. K. Shih, et al. (2000). Scanning probe-based frequency-dependent microrheology of polymer gels and biological cells. ***Phys Rev Lett***, 85, 880-3.

Maksym, G. N., B. Fabry, et al. (2000). Mechanical properties of cultured human airway smooth muscle cells from 0.05 to 0.4 Hz. ***J Appl Physiol***, 89, 1619-32.

Mijailovich, S. M., J. P. Butler, et al. (2000). Perturbed equilibria of myosin binding in airway smooth muscle: bond-length distributions, mechanics, and ATP metabolism. ***Biophys J***, 79, 2667-81.

Mijailovich, S. M., M. Kojic, et al. (2002). A finite element model of cell deformation during magnetic bead twisting. ***J Appl Physiol***, 93, 1429-36.

Murphy, R. A. (1988). muscle cells of hollow organs. ***News Physiol Sci***, 3, 124-128.

Navajas, D., S. Mijailovich, et al. (1992). Dynamic response of the isolated passive rat diaphragm strip. ***J Appl Physiol***, 73, 2681-92.

Puig-de-Morales, M., E. Millet, et al. (2004). Cytoskeletal mechanics in adherent human airway smooth muscle cells: probe specificity and scaling of protein-protein dynamics. ***Am J Physiol Cell Physiol***, 287, C643-54.

Satcher, R. L., Jr. and C. F. Dewey, Jr. (1996). Theoretical estimates of mechanical properties of the endothelial cell cytoskeleton. ***Biophys J***, 71, 109-18.

Shroff, S. G., D. R. Saner, et al. (1995). Dynamic micromechanical properties of cultured rat atrial myocytes measured by atomic force microscopy. ***Am J Physiol***, 269, C286-92.

Sollich, P. (1998). Rheological constitutive equation for a model of soft glassy materials. ***Phys Rev E***, 58, 738-759.

Sollich, P., F. Lequeux, et al. (1997). Rheology of soft glassy materials. ***Phys Rev Lett***, 78, 2020-2023.

Suki, B., R. Peslin, et al. (1989). Lung impedance in healthy humans measured by forced oscillations from 0.01 to 0.1 Hz. ***J Appl Physiol***, 67, 1623-9.

Wang, L., P. D. Pare, et al. (2001). Effect of chronic passive length change on airway smooth muscle length-tension relationship. ***J Appl Physiol***, 90, 734-40.

Wang, N., I. M. Tolic-Norrelykke, et al. (2002). Cell prestress. I. Stiffness and prestress are closely associated in adherent contractile cells. ***Am J Physiol Cell Physiol***, 282, C606-16.

Warshaw, D. M., D. D. Rees, et al. (1988). Characterization of cross-bridge elasticity and kinetics of cross-bridge cycling during force development in single smooth muscle cells. ***J Gen Physiol***, 91, 761-79.

Weber, W. (1835). Ueber die Elasticitaet der Seidenfaeden. ***Annalen der Physik und Chemie***, 34, 247-257.

Weber, W. (1841). Ueber die Elasticitaet fester Koerper. ***Annalen der Physik und Chemie***, 54, 1-18.

Yamada, S., D. Wirtz, et al. (2000). Mechanics of living cells measured by laser tracking microrheology. ***Biophys J***, 78, 1736-47.